Journal of Materials Chemistry A

Improved Storage Stability of Conjugated Polymer Solutions with a Versatile Non-Halogenated Solvent for Organic Solar Cells

Journal:	*Journal of Materials Chemistry A*
Manuscript ID	TA-ART-01-2025-000434.R1
Article Type:	Paper
Date Submitted by the Author:	21-Feb-2025
Complete List of Authors:	Chen, Ying; Xi'an Jiaotong University, State Key Laboratory for Mechanical Behavior of Materials Zhao, Zhenhan; Xi'an Jiaotong University, Centre of Nanomaterials for Renewable Energy, State Key Laboratory of Electrical Insulation and Power Equipment, School of Electrical Engineering, Zhou, Ke; Xi'an Jiaotong University, State Key Laboratory for Mechanical Behavior of Materials Jili, Ncedo; University of KwaZulu-Natal, School of Chemistry & Physics Mola, Genene; University of KwaZulu-Natal - Pietermaritzburg Campus, Physics Zheng, Hong; Xi'an Jiaotong University, Centre of Nanomaterials for Renewable Energy, State Key Laboratory of Electrical Insulation and Power Equipment, School of Electrical Engineering Ma, Wei; Xi'an Jiaotong University, State Key Laboratory for Mechanical Behavior of Materials

ARTICLE

Improved Storage Stability of Conjugated Polymer Solutions with a Versatile Non-Halogenated Solvent for Organic Solar Cells

Received 00th January 20xx,
Accepted 00th January 20xx

DOI: 10.1039/x0xx00000x

Ying Chen,[a] Zhenhan Zhao,[b] Ke Zhou,*[a] Ncedo Jili,[c] Genene Tessema Mola,[c] Hong Zheng,*[b] and Wei Ma*[a]

The progress towards the realization of organic solar cells (OSCs) as alternative energy source has made tremendous strides in recent years. The solution processability of active layers endows OSCs with several advantages, while concomitantly brings a bottleneck to their commercial application due to the instability of conjugated polymer solutions in ambient environment. Here, the key factors dominating the solution stability of conjugated polymer processed with non-halogenated solvents, Toluene and 1,2,4-Trimethylbenzene (TMB), were investigated using a prototypical polymer donor PM6. The analysis of solvent parameters shows that the relatively bigger polarity and molar volume of TMB could weaken the aggregation tendency of PM6 molecules by strengthening the solvation effect, resulting in the superior storage stability compared to the Toluene-processed solution. It is found that the unstable Toluene-processed PM6 solution can lead to the inappropriate phase separation and reduce the uniformity of the blend film, thus weakening the power conversion efficiency (PCE) of devices with the sequentially deposited PM6/L8-BO active layers. While the TMB-processed PM6 solution exhibits an excellent storage stability reaching 60 days, and the device performances based on those aged solutions are rather comparable with the devices manufactured with fresh solution. This provides a guidance for the solvent selection in the industrial production of OSCs, which will benefit the preparation, storage, and processing of active layer solutions, resembling commercially used PEDOT:PSS inks.

Introduction

Organic solar cells (OSCs) have made significant breakthroughs in device efficiency in recent years.[1,2] Notably, the design and synthesis of new conjugated polymers and small molecular donor and acceptor, along with the optimization of processing techniques, have enabled the power conversion efficiency (PCE) of single-junction devices to increase from less than 1% to over 20%[3-10]. Such progress in PCE has led OSC to be an important thin film solar cell technology. Conjugated polymer based solar cells offer not only competitive performances but also possess several other advantages, such as mechanical flexibility, tunable energy bandgaps, and lightweight, which allow OSCs to be fabricated on the flexible, stretchable, and semi-transparent substrates.[11-13] Consequently, numerous potential applications are reported for OSCs in fields of wearable electronic, building-integrated photovoltaics (BIPV), and drone energy supply systems.[14-16] More importantly, the solution processability of conjugated polymer provides OSCs with advantages for large-area production through rapid solution-based printing methods, which effectively simplifies the preparation process for active layers and lays a foundation for reducing costs.

Many researchers have found that the solution state of active layer is important to determining the device performance of OSCs. The degree of molecular entanglement of conjugated polymer, the size of the aggregates and other parameters in the solution can regulate the morphological structure of the active layer film, such as the domain size, purity and crystallinity, which will be closely related to the exciton dissociation and charge transport efficiency of the device.[17-21] Currently, the active layer of OSCs is predominantly processed using freshly prepared solution that allows high polymers miscibility and optimized film morphology, however, the molecular aggregation will undergo changes upon aging the solutions. Interestingly, Wang *et al* found that the aggregation effect of conjugated polymer can be employed to enhance the crystallinity of the film, which appropriately contributes to the improved charge transport and collection efficiency in the devices.[22] On the other hand, for most conjugated polymers, prolonged solution aging time leads to an increase in viscosity. When a green non-halogenated solvent is used to prepare the active layer solution, the viscosity rapidly changes with aging, resulting in a significant deterioration in the uniformity of the printed films and thus the reduced device performance. This

[a] State Key Laboratory for Mechanical Behavior of Materials, Xi'an Jiaotong University, Xi' an 710049, China E-mail: msekzhou@xjtu.edu.cn (K. Zhou), msewma@xjtu.edu.cn (W. Ma).
[b] Centre of Nanomaterials for Renewable Energy, State Key Laboratory of Electrical Insulation and Power Equipment, School of Electrical Engineering, Xi'an Jiaotong University, Xi'an 710049, China, E-mail: zhenghong666@xjtu.edu.cn.
[c] School of Chemistry & Physics, University of KwaZulu-Natal, Pietermaritzburg Campus, Private Bag X01, Scottsville, Pietermaritzburg 3209, South Africa.
Electronic Supplementary Information available: Details of experiments and calculations; supplementary figures, supplementary tables, and supplementary references. See DOI: 10.1039/x0xx00000x.

suggests that the conjugated polymer molecules have a strong aggregation tendency in solution due to the π-π interactions, which leads to the thermodynamic instability of the active layer solution and seriously limits the window time for the storage, transportation, and processing of the active layer solution in an industrial large-scale production of OSCs.

Currently, both the active layer and interface layer of OSCs need to be processed using solution methods. Most freshly prepared active layer solutions remain stable not for more than few hours in ambient environment.[23,24] Meanwhile, the hole transport layer solutions (such as PEDOT:PSS) can typically be stored stably for over three months, while electron transport layer solutions (including PFN-Br and PDINO) can maintain stable for more than a week. Recently, Liu *et al*. found that the BBL:PCAT-K electron transport layer solutions can exhibit even greater stability for up to six months, demonstrating the excellent processing convenience.[25] Therefore, compared to the interface layer solutions, enhancing the storage stability of active layer solutions has become a critical scientific challenge in achieving the industrial scale production of OSCs. However, the key solvent parameters and processing techniques to improve the solution stability for OSCs still remain unclear.[27,28] This uncertainty arises from the insufficient understanding of the mechanisms on the aggregation behaviors of conjugated polymers that leads to poor solution stability, particularly for the Donor-Acceptor (D-A) type conjugated polymers with relatively rigid backbones.

This work investigated the key factors dominating the solution stability of a prototypical polymer donor PM6 processed with non-halogenated solvents, Toluene and TMB, and analyzed the effect of solution stability on the device performance. Viscosity tests and cryo-electron microscopy results indicate that the solution state of Toluene-processed PM6 is rather unstable, with molecules tending to form self-aggregation when solution aged for 48 hours. While the TMB-processed PM6 solution exhibits an excellent stability under the same conditions. Interaction energy analysis and solvent parameter tests reveal that the solvent polarity and molar volume are the critical parameters influencing the storage stability of PM6 solution. The effect of solution stability on device performance was studied by sequentially depositing the non-fullerene acceptor L8-BO on the PM6 layers processed from different aged solutions. It was found that the average PCEs of Toluene-processed devices will decrease from 17.20% to 13.99% with the storage time of PM6 solution extending to 48 hours, while the TMB-processed devices show the comparable PCEs around 16.96%, which is independent of the storage time of PM6 solution. When the solution concentration decreases from 7 to 3 mg mL^{-1}, the stable storage time of TMB-processed PM6 solution can reach an excellent value of 60 days. It was found that the inappropriate phase separation during depositing L8-BO solutions on top of the Toluene-processed PM6 layers can be observed when using the aged PM6 solutions, leading to the undesirable morphology with inhomogeneous domain size in the blend films and thus the inferior device performance. Interestingly, the similar PCE variations can also be observed when using the mixed L8-BO and BTP-ec9 as acceptors, which exhibit the stable values of 18.02% for the TMB-processed devices and the discrepant values ranging from 18.04% to 15.77% for the Toluene-processed devices after aging for 48 hours. Furthermore, the solvent-dependent solution stability for another two polymer donors PTQ10 and PCE10 was also investigated, and the better solution stability and device performance when using TMB can be identified, confirming that TMB can universally improve the solution stability of polymer donors. Therefore, this work provides evidence on the aging process of active layer solutions and proposes a guidance for the solvent selection in industrial production of OSCs, which will benefit the preparation, storage, and processing of active layer solutions.

Results and discussion

The prototypical D-A type donor PM6 was chosen as a reference system to investigate the key factors influencing the storage stability of conjugated polymer solutions. The chemical structures of PM6 and non-halogenated processing solvents, Toluene and TMB, are shown in Fig. 1a. The PM6 solutions were prepared with two solvents at the concentrations of 3, 5, and 7 mg mL^{-1}, respectively, which are reported to be the suitable solution concentrations for printable processing.[26] Those solutions were kept at room temperature and aged for different time, namely freshly prepared (0 h), aged for 24 hours (24 h) and 48 hours (48 h), and then followed by the measurements of their solution viscosities to evaluate their storage stability. As shown in Fig. 1b-c and Table S1, ESI, the viscosity of the PM6 solution at a concentration of 3 mg mL^{-1} remains relatively unchanged over time when Toluene is used as the solvent. In contrast, the viscosity of the solution at a concentration of 5 mg mL^{-1} shows a slight increase upon aging, and a significant rise in viscosity from 36.89 to 98.57 mm^2 s^{-1} can be observed in the solution at a concentration of 7 mg mL^{-1}. On the other hand, with TMB as the solvent, the solutions of all tested concentrations show negligible changes in viscosity over time. This suggests that PM6 solutions prepared with Toluene exhibit greater susceptibility to increase in viscosity during aging compared to those prepared with TMB, suggesting poor storage stability.

Subsequently, we characterized the microscopic state of PM6 molecules within these solutions with the concentration of 7 mg mL^{-1} by using freeze drying techniques.[27] The atomic force microscope (AFM) and transmission electron microscope (TEM) images are provided in Fig. 1d-g and Fig. 1h-k, respectively. When Toluene is used as the solvent, PM6 molecules predominantly form the lamellar aggregates with a globular shape. In contrast, when TMB serves as the solvent, those PM6 molecules primarily develop into the branch-like aggregates with smaller domain size.[28] This indicates that PM6 shows enhanced solubility in TMB than in Toluene. Comparing Fig. 1d, e with 1h, i the significantly increased aggregate size in the Toluene-processed PM6 solutions was observed after aging for 48 hours. Nevertheless, Fig. 1f, g and 1j, k demonstrate the rare change in aggregate size when using TMB as the solvent. These

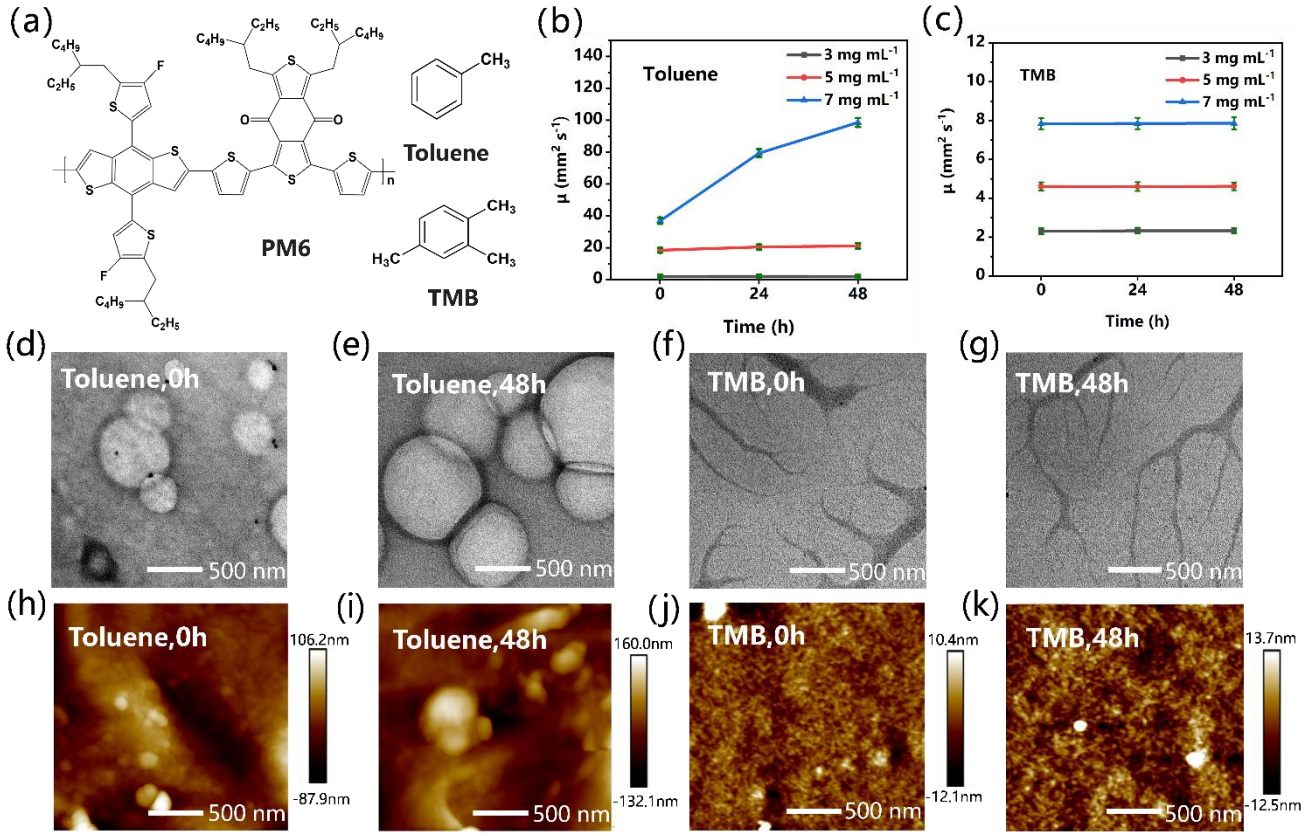

Fig. 1 (a) Chemical structures of PM6, Toluene, and TMB. (b and c) The viscosity of solutions with Toluene and TMB as solvents at different concentrations and for different aging times. (d-g) Freeze drying TEM and (h-k) AFM images of PM6 solutions for the freshly prepared and aged for 48 hours at room temperature when using Toluene and TMB as the solvents.

suggest that PM6 molecules tend to self-aggregation more readily when dissolved in Toluene, while their aggregation state remains largely unchanged in TMB solvent, suggesting a better stability of TMB based solutions.

Furthermore, the morphology of PM6 films prepared from solutions of different aging time were investigated using AFM. As shown in Fig. S1, ESI, it can be observed that the aggregation size in the Toluene-processed film increased significantly after aging for 48 hours, with the root mean square roughness (RMS) values increased from 1.5 to 2.9 nm. On the other hand, no evident change of aggregation was observed from TMB solvent based films, and the RMS values kept constant around 1.5 nm. This suggests that enhanced aggregation of PM6 molecules in Toluene based solutions is persistent even in solid phase as observed from corresponding films. The phenomenon of enhanced aggregation after aging has also been reported in previous study,[23] which shows PM6 solution in chloroform exhibited pre-aggregation after cold-aging, leading to an increased aggregation in the thin films. The crystallinity and molecular orientation of the films were further investigated using grazing incidence wide angle x-ray scattering (GIWAXS), and the results are provided in Fig. S2, ESI. The interplanar spacing (D-spacing) and crystalline coherent length (CCL) are quantified based on the GIWAXS image employing the Bragg's Law and Scherrer equation,[29,30] the fitted data are summarized in Table S2, ESI. When Toluene is used as the solvent, it shows an increase of the CCL for the in-plane (*010*) and out-of-plane (*100*) peaks while a decrease is observed for the in-plane (*100*) and out-of-plane (*010*) peaks, suggesting a molecular packing variation from face-on to edge-on. In contrast, no significant changes are noted in either aggregation or molecular orientation for the TMB-processed films. The paracrystallinity (*g*) of those films was also analyzed based on the Equation 1,[31] where Δq and d_{hkl} are the full width at half maximum (FWHM) and the interplanar spacing of the diffraction peak of interest, respectively.

$$g = \frac{1}{2\pi}\sqrt{\Delta q * d_{hkl}} \quad (1)$$

The results are summarized in Table S3, ESI. The TMB-based PM6 films show the similar paracrystalline disorder after aging. However, the Toluene-based PM6 films exhibit a decreased paracrystalline disorder (from 13.46% to 11.83%) for the in-plane *(010)* peak and an increased paracrystalline disorder (from 14.09% to 16.85%) for the out-of-plane *(010)* peak after aging 48 hours, suggesting the more disordered packing in the face-on orientation. Obviously, the GIWAXS results are consistent with the AFM images, both confirming that the instability of Toluene-processed solution leads to an increase in aggregation within the film, whereas TMB-processed solution is relatively stable, resulting in minimal changes to the morphology of the film.

Furthermore, the mechanism that influences the storage stability of PM6 solutions prepared from different solvents was

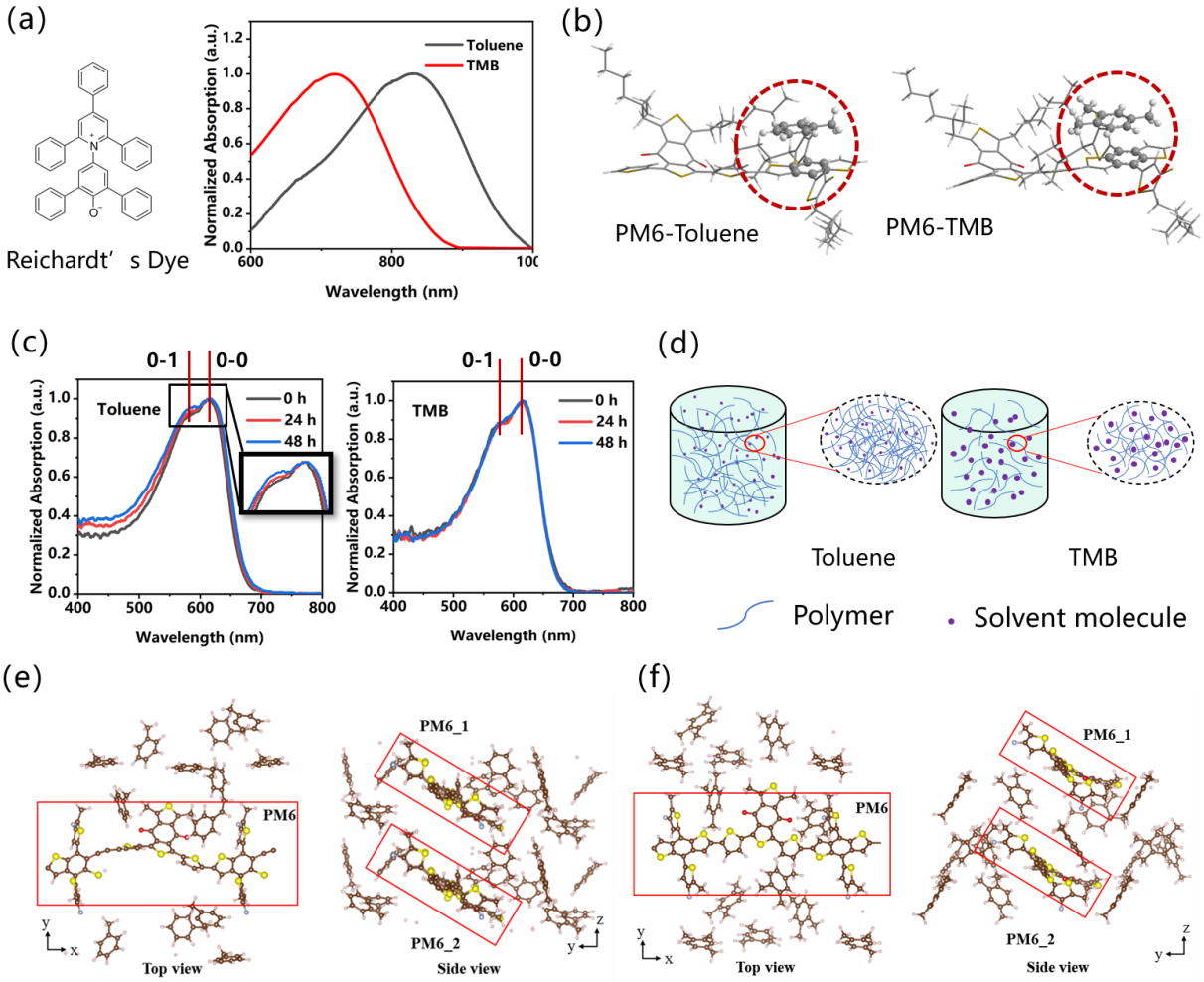

Fig.2 (a) The chemical structure of Reichardt's dyes and UV-vis absorption spectra of Reichardt's dyes in two solvents. (b) The main form of combination between PM6 and solvent molecules in solution. (c) The UV-vis absorption spectra of the solutions in different aging time. (d) The schematic representation of PM6 molecules in Toluene and TMB. Configuration of simplified PM6 in (e) Toluene and (f) TMB after 6 ps simulation.

also studied. According to Hansen solubility parameter theory, the solubility of a solute in a solvent is primarily related to the molar volume of the solvent and the interaction between the solute and solvent molecules.[32] First, we measured the polarity parameter $E_T(30)$ of solvents, which is characterized by electronic transition energies obtained from the UV-Vis absorption spectra of Reichardt's Dye in various solvents.[33-35]This polarity parameter reflects the interactions within the solvation shell surrounding the solute and embodies the overall dissolving capability of the solvent. The UV-Vis spectra for Reichardt's Dye in two different solvents are illustrated in Fig. 2a. Based on calculations from their maximum wavelengths, we find that $E_T(30)$ values for Toluene and TMB are 34.45 and 40.16 kcal mol^{-1}, respectively. Compared to Toluene, a higher $E_T(30)$ value for TMB indicates its superior overall solubility.

In order to make the measured polarity parameter $E_T(30)$ more convincing, the interactions between PM6 and Toluene/TMB were also calculated theoretically so as to analyze the key differences between these solvents. As illustrated in Fig. S3, ESI, the interactions between PM6 and two solvent molecules may involve four configurations: the π-π stacking of carbon-carbon double bonds between the PM6 molecule and solvent molecule, the π-π stacking of carbon-carbon double bonds (PM6 molecule) and carbon-sulfur double bonds (solvent molecule), the hydrogen bonds between H atoms (solvent molecule) and O atoms (PM6 molecule), and the hydrogen bonds between H atoms (solvent molecule) and F atoms (PM6 molecule). Among the four configurations, the binding energy of the π-π stacking between carbon-carbon double bonds is comparatively lower, indicating that the interaction between PM6 and solvent molecules in solution is mainly due to the π-π stacking of carbon-carbon double bonds (Fig. 2b). In this configuration, the binding energies of PM6 with Toluene and TMB are -16.7 and -20.7 kcal mol^{-1}, respectively. The higher binding energy suggests the stronger interaction between PM6 and TMB molecules, which will strengthen the solvation effect and promote the stability of PM6 molecules in TMB. Additionally, the quantum chemical method is applied to analyze the origin of binding energies, which can be broadly categorized into four components: the classical electrostatic interaction energy ΔE_{els} which reflects the electron-nucleus interactions, the exchange-repulsion term ΔE_{xrep} which

Table 1. The results of binding energy analysis by quantum chemistry method

Type	Binding energy/Kcal	ΔE_{els} /Kcal	ΔE_{xrep} /Kcal	ΔE_{orb} /Kcal	ΔE_c /Kcal
PM6-Toluene	-16.7	-6.4	11.5	-5.5	-16.4
PM6-TMB	-20.7	-8.2	14.5	-6.3	-20.7

represents the electron-electron interactions, the orbital interaction energy ΔE_{orb} which indicates a certain degree of overlap between molecular orbitals, and the coulomb correlation terms ΔEc which accounts for the weak intermolecular forces, such as van der Waals force. The magnitudes of each type of interaction are summarized in Table 1. The predominant force governing the interaction between PM6 and Toluene/TMB can be attributed to the van der Waals force, which nearly equates to their overall binding energies. The higher polarity of TMB likely enhances the polarization effects on PM6 and thus leads to the stronger van der Waals interactions, which is primarily responsible for its greater binding energy compared to Toluene.

The UV-vis absorption spectra of the solutions were subsequently measured so as to analyze the effect of the molar volume of solvent on the solution stability. As shown in Fig. 2c, the ratio of the 0-1 to 0-0 peaks reflects the degree of H-type aggregation.[36] When Toluene is used as the solvent, the H-type aggregation of PM6 in the solution increases after aging, indicating an enhancement in the intermolecular π-π stacking, while there are no significant changes observed for the TMB-processed solutions. This may be attributed to the larger molar volume of TMB, which increases the steric hindrance and weakens the π-π interactions between the adjacent polymer molecules. On the other hand, the first-principles molecular dynamics (AIMD) was used to simulate the kinetic behavior of the simplified PM6 solute molecule in two solvents, Toluene and TMB. To explore the π-π stacking between solute and solvent molecules, we have simplified the molecular configuration of PM6, whose marginal side chains are replaced with methyl groups and main chain is periodically extended along the x-axis, as shown in Fig. S4a, ESI. Fluctuations of total energy in Toluene and TMB during AIMD simulation are shown in Fig. S4b, c, ESI. In Toluene solvents, the Toluene molecules between the upper and lower PM6 chains tend to move to both sides of the y-axis, and the lattice constant *c* shrinks from 12 to 10.8 Å. The vertical distance between two PM6 chains is approximately 6.3 Å. However, in TMB solvents, some of the solvent molecules are still retained between the upper and lower PM6 chains. Moreover, the lattice constant *c* has a slightly increasing, from 12 to 12.4 Å. The vertical distance between two PM6 chains is approximately 7.8 Å. The final configuration results are shown in Fig. 2e, f. The relatively bigger vertical distance confirms that the TMB molecules can inhibit the aggregation of PM6 molecules due to their larger molar volume, which is consist with the results of UV-vis absorption spectra. According to the aforementioned analysis, which comprises theoretical calculations and experimental methodologies, the schematic representation of PM6 molecules in Toluene and TMB is presented in Fig. 2d. The smaller solvent polarity parameter and molar volume of Toluene facilitate the self-aggregation of PM6 molecules, while the larger solvent polarity parameter combined with a relatively greater molar volume of TMB enhances the solubility of PM6 molecules, resulting in a more stable solution.

Subsequently, we investigated the impact of solution stability on the device performance of OSCs. L8-BO is a commonly used high-efficiency acceptor with its chemical structure shown in Fig. 3a. Using PM6 as the donor material, the devices based on the sequentially blade-coated active layers were prepared (as presented in schematic diagram Fig. 3b). PM6 and L8-BO exhibit the compatible energy levels and absorption spectra, as shown in Fig. S5c-d, ESI, ensuring minimal energy loss and sufficient driving force for exciton dissociation. First, the solution stability of L8-BO was investigated at a concentration of 10 mg mL^{-1} by conducting the viscosity tests and measuring the UV-vis absorption spectra at room temperature. As shown in Fig. S5a-b, ESI, no significant changes can be observed for those L8-BO solutions after aging. It suggests that this solution possesses good stability, allowing us to rule out any influence of the acceptor solution stability on device performance in subsequent analysis. The current density-voltage (*J-V*) curves and external quantum efficiency (EQE) of OSCs prepared by Toluene-based PM6 solutions that are not aged, aged for 24 hours and 48 hours are shown in Fig. 3c and S6a, ESI, respectively. The specific photovoltaic parameters are summarized in Table 2. Compared to the devices fabricated without solution aging, the PCEs of the devices fabricated with the solutions aged for 24 and 48 hours decreased from 17.06% to 15.28% and then to 13.89%, respectively, with other photovoltaic performance parameters also showing varying degrees of decline. It demonstrates that the instability of the PM6 solution leads to a deterioration in the optoelectronic performance of the resulting devices. This conclusion aligns with previous study,[24] where the PCE of PM6:BTP-BO-4Cl OSCs device decreased from 15.69% to 12.59% after the solution was aged for 120 minutes.

We conducted an analysis of the physical processes in the device, beginning with the measurement of photogenerated current density-effective voltage (J_{ph}-V_{eff}) curve (Fig. S6b, ESI). The exciton dissociation efficiency can be obtained by analyzing the charge dissociation and extraction process,[37] as shown in Fig. S6c, ESI. The exciton dissociation efficiency gradually decreases with prolonged solution aging, dropping from 95.3% to 93.4%, and then to 93.0%. This indicates that the instability of the PM6 solution adversely affects the exciton dissociation efficiency, leading to a reduction in short-circuit current density (J_{SC}) and fill factor (FF). Then, the curves of the J_{SC} and open-circuit voltage (V_{OC}) varying with light intensity were tested, as shown in Fig. S6d, ESI, and Fig. 3e. There is a linear relationship between V_{OC} and the natural logarithm of light intensity. The

Table 2. Photovoltaic parameters of PM6/L8-BO OSCs with different aging time under illumination of AM 1.5G at 100 mW cm^{-2}

Condition	V_{OC} (V)	J_{SC} (mA cm^{-2})	FF (%)	PCE (%)[a]
Toluene, 0 h	0.867	25.52	77.01	17.06 ± 0.16 (17.20)[b]
Toluene, 24 h	0.858	23.49	73.34	15.28 ± 0.41 (16.23)
Toluene, 48 h	0.855	22.32	71.94	13.89 ± 0.73 (16.02)
TMB, 0 h	0.862	25.23	77.25	16.85 ± 0.17 (16.98)
TMB, 24 h	0.864	25.34	77.19	16.78 ± 0.23 (16.95)
TMB, 48 h	0.865	25.32	77.32	16.72 ± 0.19 (16.91)

a The average PCEs are obtained from 10 devices.

b The maximum value of PCE is shown in the bracket.

slope of the curve obtained by fitting can further analyze the defect state recombination (SRH) inside the device. The closer the slope S to 1, the lower degree of the defect state recombination in the device.[38] In addition, there is a linear relationship between J_{SC} and the natural logarithm of light intensity $J_{SC} \propto P^{\alpha}$, and the closer the α value to 1, the weaker the bimolecular recombination of the device.[39] The slope fitting results show that the defect state recombination of the device increases after solution aging, but the bimolecular recombination degree does not change significantly. The increased defect state recombination degree is probably one reason for the deterioration of PCE in the Toluene-processed devices.

Similarly, the sequentially deposited devices based on the TMB-processed PM6 solutions that are not aged, aged for 24 hours and 48hours were also manufactured, and the corresponding *J-V* curves and EQE curves of the devices are shown in Fig. 3d and S7a, respectively. The specific photovoltaic performance parameters are summarized in Table 2. The PCEs of the devices have no obvious change before and after the aging of PM6 solution, which all exhibit a rather comparable value of 16.78%. This confirms the good stability of the PM6 solution using TMB solvent. The physical process of the device is also analyzed, as shown in Fig. 3f and S7b-d. The exciton dissociation efficiency of the device is basically unchanged before and after solution aging (around 92.8%), and the degree of charge recombination does not change significantly, which is consistent with the nearly same photoelectric performance of the device.

The carrier mobility of the device was tested using the Space Charge Limited Current (SCLC) model.[40,41] The $J^{1/2}$-V characteristics of devices are shown in Fig. S8, ESI. The charge transport parameters were derived from the curve fitting with transport equations, which are given in Fig. 3g-f and summarized in Table S4, ESI. According to the results obtained

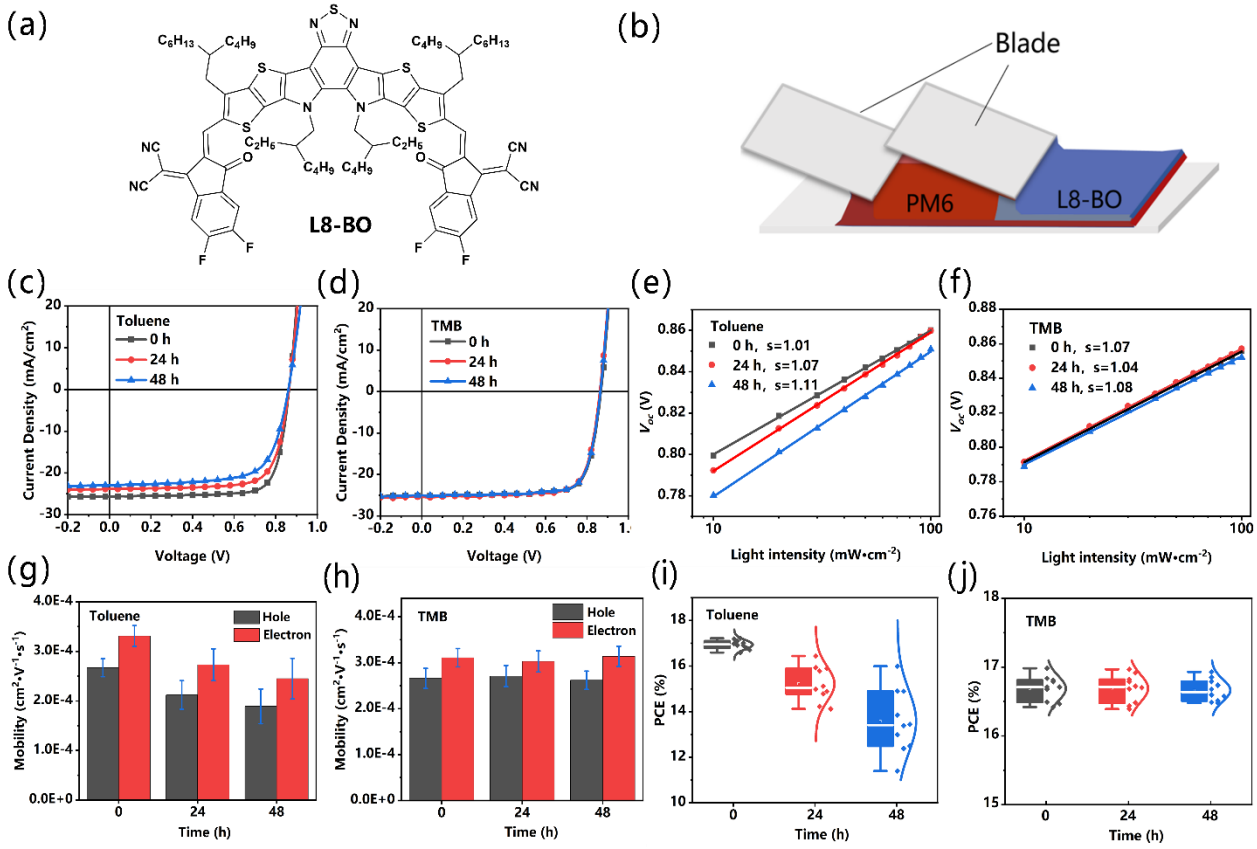

Fig.3 (a) Chemical structure of L8-BO. (b) Schematic diagram of blade coating. (c, d) *J-V* curves, (e, f) VOC-Light intensity curves, (g, h) carrier mobilities, and (i, j) efficiency distribution diagram of PM6/L8-BO OSCs with Toluene/TMB being the solvent of PM6.

from Toluene based PM6 devices, both hole and electron mobilities gradually decrease (from 2.67×10^{-4} to 1.79×10^{-4} cm^2 V^{-1} s^{-1}, and from 3.31×10^{-4} to 2.45×10^{-4} cm^2 V^{-1} s^{-1}, respectively) with prolonged solution aging time. Conversely, in TMB based devices, there are no significant changes observed in either hole or electron mobilities over time (nearly 2.72×10^{-4} cm^2 V^{-1} s^{-1} and 3.14×10^{-4} cm^2 V^{-1} s^{-1}, respectively). It indicates that the instability of PM6 solution adversely affects the charge transport properties of the devices. Furthermore, the uniformity of device performance was statistically analyzed for each processing condition. As shown in Fig. 3i, j, it is observed that with prolonged solution aging time the overall efficiencies of the devices gradually decrease and the distribution of PCE becomes more dispersed for Toluene based OSC. In contrast, as the solution solvent changed to TMB, no significant variation is noted for the PCE distribution despite extending the aging time, which means the instability of PM6 solutions will inhibit the uniformity of device performance.

The aforementioned results indicate that the instability of the PM6 solution can lead to a decline in device performance. To explain the underlying reasons, a detailed analysis of the film morphology is necessary. The optical microscope images and UV-vis absorption spectra of the sequentially deposited PM6/L8-BO films were measured at four uniformly spaced regions along the direction perpendicular to blade coating. As shown in Fig. 4a, when Toluene is used as the solvent, there are no significant differences in optical images for PM6/L8-BO films made from the solutions that have not been aged and the absorption spectra across various regions overlap considerably with minimal component fluctuations. However, after the solution was aged for 48 hours, the variations in optical images indicate the fluctuations in film thickness across different regions. The normalized absorption spectra exhibit substantial differences at the wavelength ranging from 400 to 700 nm, which mainly resulted from the donor materials. This suggests that the ratio of donor/acceptor (D/A) at certain regions deviates from its average value, leading to the considerable variability in component distribution in the whole PM6/L8-BO film. This fluctuation may be attributed to a significant increase in viscosity of PM6 solution upon aging using Toluene as solvent. The increased viscosity likely leads to an uneven distribution of solution between substrate and blade during coating and thus results in non-uniform thickness in the solid film. After depositing the L8-BO solution on top of the heterogeneous PM6 layers, the D/A ratio will vary from the average values. Such variability in component distribution can obviously restrict the charge separation, transport, and collection processes, totally contribute to the discrete PCE. On the other hand, when TMB is used as the solvent, the optical microscope images and UV-visible absorption spectra for the films without and with solution aging show no notable changes, suggesting a favorable uniformity regarding film thickness and component distribution in the TMB-processed PM6/L8-BO films.

The surface morphology of the films was characterized using AFM, and the AFM height images are provided in Fig. S9,

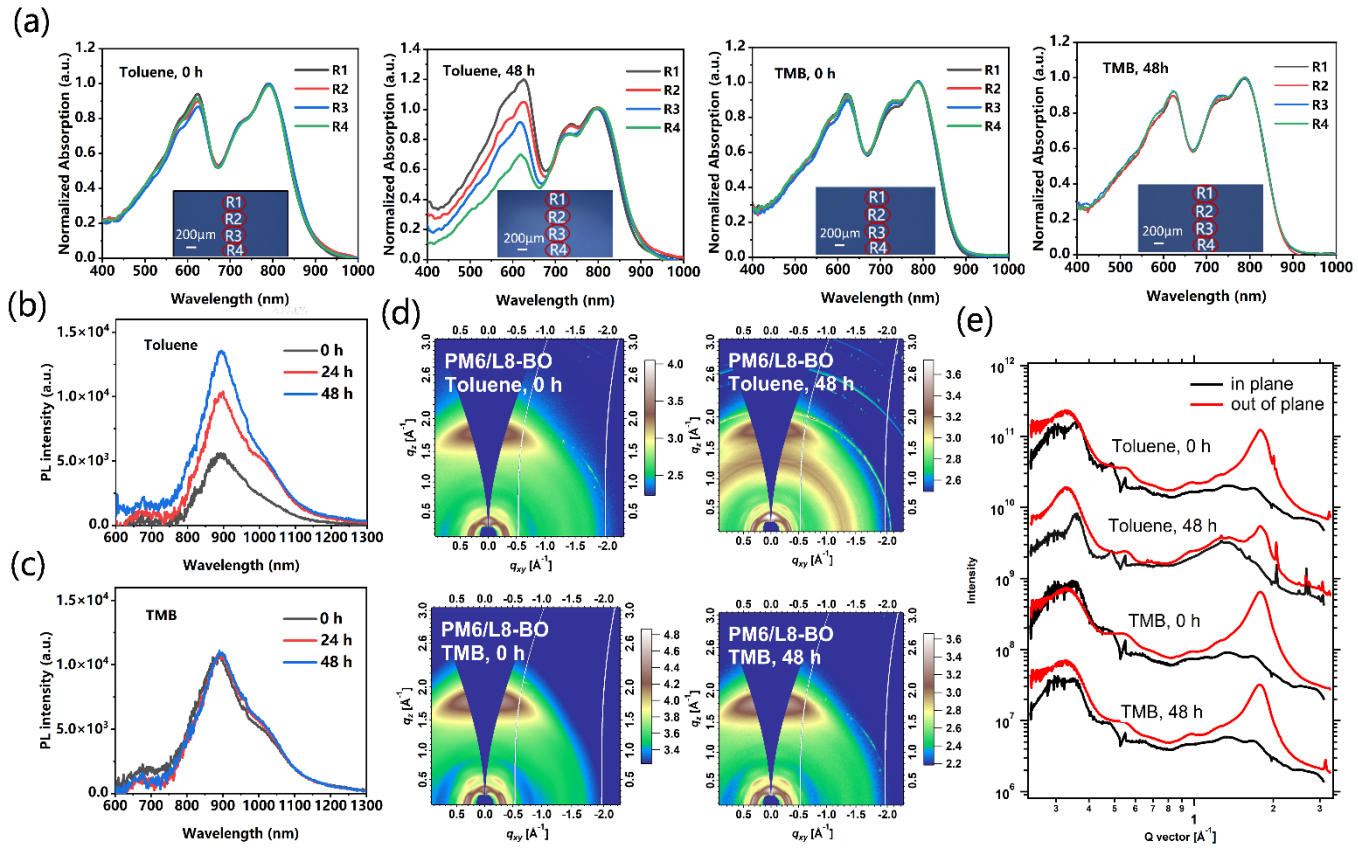

Fig.4 (a) Optical microscope images and UV-visible absorption spectra at four uniformly spaced regions of PM6/L8-BO films. (b, c) PL spectra of the PM6/L8-BO films under different aging time. (d) 2D GIWAXS patterns and (e) the corresponding line profiles of the PM6/L8-BO films.

ESI. There is no significant difference in the surface morphology of PM6/L8-BO films prepared from two different solvents after aging the solution for 48 hours. Further testing of the photoluminescence (PL) spectra of the films, as shown in Fig. 4b, revealed that in Toluene based devices, an increase in solution aging time leads to an enhancement in PL intensity and a decrease in quenching efficiency of the photo-induced charges. This is an indication of the presence of large aggregates in the film that reduces D/A interfacial area, which inevitably reduce the device performance. The quenching efficiency of the film remains relatively unchanged (Fig. 4c) upon aging in the case of TMB based solution, suggesting a relatively homogeneous distribution of donor and acceptor domains in the PM6/L8-BO films. Besides, the two-dimensional (2D) GIWAXS patterns and line profiles of the PM6/L8-BO films obtained before and after solution aging are presented in Fig. 4d-e. The film has the strong (*010*) scattering peaks at q = 1.76 $Å^{-1}$ in the out-of-plane direction (attributed to both PM6 and L8-BO), revealing a face-on orientation. Meanwhile, there exist the (*100*) peaks at q = 0.29 $Å^{-1}$ (highly attributed to PM6) and q = 0.36 $Å^{-1}$ (highly attributed to L8-BO) in the in-plane direction. The D-spacing and CCL values extracted from the line profiles are summarized in Table S5, ESI. The results of the fitting indicate that the CCL of the (*010*) peaks in the out-of-plane direction improves significantly after solution aging (from 21.36 to 24.15 nm) in the Toluene based films. In contrast, no significant changes in the D-spacing and CCL are observed in the case of TMB solvent. This is consistent with the earlier hypothesis that the aggregation within the PM6 solution can be retained in the film, reflected in the peak location and FWHM in the GIWAXS images.

To investigate the impact of the stability of active layer solutions on device performance, optical measurements were conducted using *in situ* UV-vis and *in situ* PL, to understand the behaviour of polymers aggregates from solution to solid thin film (the illustration diagram is shown in Fig. 5a).[42,43] Fig. S10, S11, ESI and Fig. 5b, c show the contour plots and spectra of *in situ* UV-vis absorption and the time evolution of L8-BO peak location under different aging time, respectively. The transition from solution to thin film can be broadly divided into three stages: solvent evaporation (blue region), aggregation transformation (yellow region), and film formation (purple region). The peak location of L8-BO remains constant over time

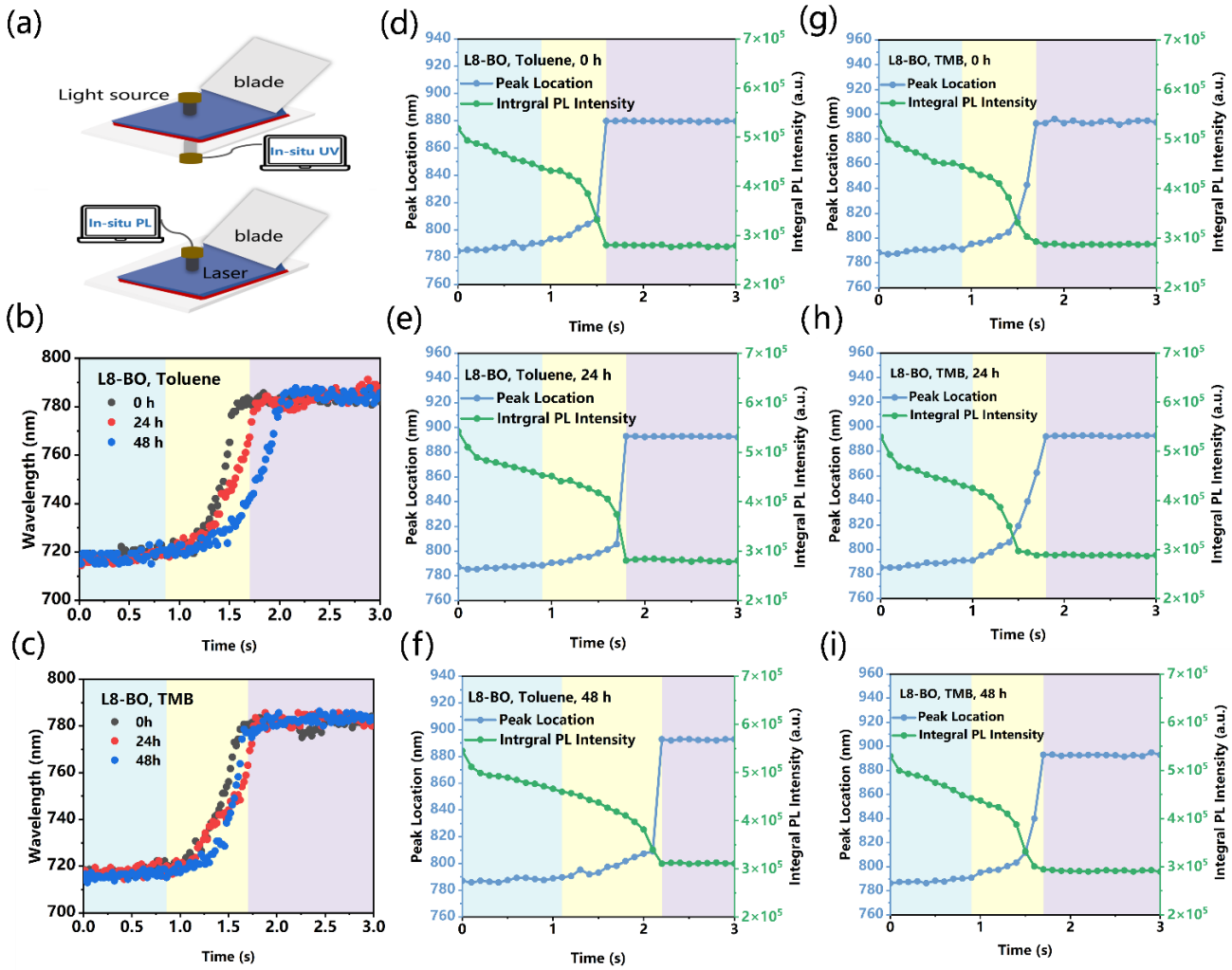

Fig.5 (a) Illustration diagram of *in situ* UV–vis absorption and *in situ* PL measurements. Time evolution of L8-BO peak location extracted from *in situ* UV-vis absorption spectra when (b) Toluene and (c) TMB are used as the solvents. Time evolution of L8-BO peak location and PL integral intensity extracted from the *in situ* PL spectra of the process from (d-f) Toluene- and (g-i) TMB-based solutions to films.

at the beginning of solvent evaporation. During the aggregation transformation stage, a redshift in peak position is observed, indicating that molecular aggregation begins as it transforms from a liquid phase to a solid phase. When the redshift of L8-BO absorption peak stops, it means the solid film has formed and the peak location of L8-BO remains constant over time. In the case of Toluene based solution, an increase in aging time leads to an elongation of L8-BO's aggregation transition time (from 0.72 to 0.86 and 1.04 s) along with a slight redshift of the absorption peak, suggesting a gradual decrease in molecular aggregation rate and a subtle improvement in degree of molecular aggregation during the transition from solution to thin film. For TMB based solution, L8-BO's aggregation time remains relatively constant (~0.85 s) regardless of the increased aging time. Thus, no significant changes are observed during its transition from solution to thin film. The results obtained through *in situ* UV-vis spectroscopy further confirm that in Toluene based solution, enhanced intermolecular aggregation within PM6 solutions is retained upon forming films. This probably inhibits the penetration of L8-BO solution into the PM6 layers and thus contributes to the extended aggregation transition time of L8-BO. Therefore, the relatively increased duration time of the phase separation between PM6 and L8-BO molecules largely results in the uneven component distribution and inferior morphology in the PM6/L8-BO films processed with aged Toluene solutions.

The quenching dynamics during the transition from solution to solid film at different aging time was investigated using *in situ* PL spectroscopy measurement. The *in situ* PL contour maps and spectra of the active layer cast from the PM6 solutions with various aging time are shown in Fig. S12, S13, respectively. Fig. 5d-f and 5g-i illustrate the time evolution of the L8-BO peak location and PL integral intensity of the samples based on the Toluene- and TMB-processed PM6 layers. The film deposition process can be categorized into three stages that correspond to those observed in the *in situ* UV-vis spectra. In Toluene based solution, an increase in solution aging time leads to a gradual extension of the film formation time (from 0.7 to 0.9 and 1.0 s). This indicates that the enhanced molecular aggregation in PM6 layer inhibits the mixing of PM6 and L8-BO, thereby promoting the molecular aggregation of L8-BO. Consequently, an increased degree of phase separation would take place in the photoactive layer, which is supported by the phenomena observed in *in situ* UV-vis spectra tests. Excessive phase separation in the active layer may lead to a decline in device performance, as confirmed by the PCE variations list in Table 2. For TMB based solution, the aggregation formation time in solid film remains relatively constant throughout the process (~0.8 s), which means the process of transition from solution to film remains unchanged. Therefore, the TMB-processed PM6/L8-BO morphology remains consistent after solution aging, which promotes the uniformity of PCEs.

Next, we analyzed the universality of TMB-induced stable solution in manufacturing efficient devices in terms of solution concentration and the variation of donor and acceptor materials. The efficiency comparisons in the devices based on the Toluene/TMB-based PM6 solutions at a concentration of 7 mg mL^{-1} have been previously conducted, in which aging for 48 hours will lead to the PCE decline in the Toluene-processed devices. In order to clarify whether the storage stability can be further prolonged by reducing solution concentration, several devices were fabricated with 3 mg mL^{-1} PM6 solutions that aged at different times. The *J-V* curves and specific photovoltaic parameters of PM6/L8-BO devices are shown in Fig. S14a-b and Table S6-7, ESI, respectively. The distribution of the measured PCE as depicted in Fig. 6b provides clear evidence of the performance of the devices. In the case of TMB based solutions, there are no significant changes in PCEs and the values are distributed around ~16.49%, which is consistent up to two months aging time. This is a clear demonstration of the exceptional stability of PM6 solutions. However, when Toluene is used as the solvent, the PCEs dramatically decrease with the aging time beyond 48 hours (from 16.52% to 13.91%), and the efficiency distribution becomes more dispersed, which indicates that the Toluene-processed PM6 solution, even at low concentration of 3 mg mL^{-1}, is still unstable when further prolongs the storage time.

Independent investigations were also conducted to confirm whether changing acceptor materials will affect the stability of TMB-processed devices. Here, the mixed acceptors L8-BO: BTP-ec9 were used to prepare the active layers and their chemical structures are shown in Fig. 6c. The *J-V* curves and the measured photovoltaic parameters of PM6/L8-BO: BTP-ec9 OSCs that are aged for different times are shown in Fig. S14c, d and Table S8, ESI. From the profiles of PCE distribution (Fig. 6d), the Toluene-processed devices exhibit a continuous decline in efficiency over aging time (from 17.95% to 16.82% and 15.77%), whereas the devices based on TMB solutions maintain the relatively stable PCE after aging (~17.92%). This demonstrates the potential application of TMB-induced stable solutions in the industrial production of OSCs regardless of the kind of acceptor materials. Among all these devices, the PCE of the champion cell is 18.04%, with *J-V* curve and EQE curve shown in Fig. S14c (0 h) and S16, ESI. Finally, we explored whether the storage stability of TMB-processed solutions can also be improved when using other polymer donors, such as PTQ10 and PCE10 (their chemical structures are shown in Fig. 6e and 6g). The *J-V* curves and PCE distributions for the devices based the donor solutions aged for different times are shown in Fig. S15, ESI and 6f, h respectively. The specific photovoltaic parameters of OSCs are summarized in Tables S9, S10, ESI. Regardless of whether PTQ10 or PCE10 serves as donor in Toluene based solutions, an increase in aging time leads to the continuous decrease in PCEs along with greater dispersion in their distributions (from 16.31% to 14.96 and 14.04% for PTQ10, and from 10.86% to 10.54% and 10.22% for PCE10). Conversely, by extending the aging time for the TMB-processed solutions, the fabricated devices show negligible changes in either PCEs or its distributions (about 16.32% and 10.88% for PTQ10 and PCE10, respectively). This indicates that both PTQ10 and PCE10 solutions exhibit instability when dissolved in Toluene while demonstrate favorable stability in TMB. This further confirms the solvent polarity and molar volume are the key factors to generally

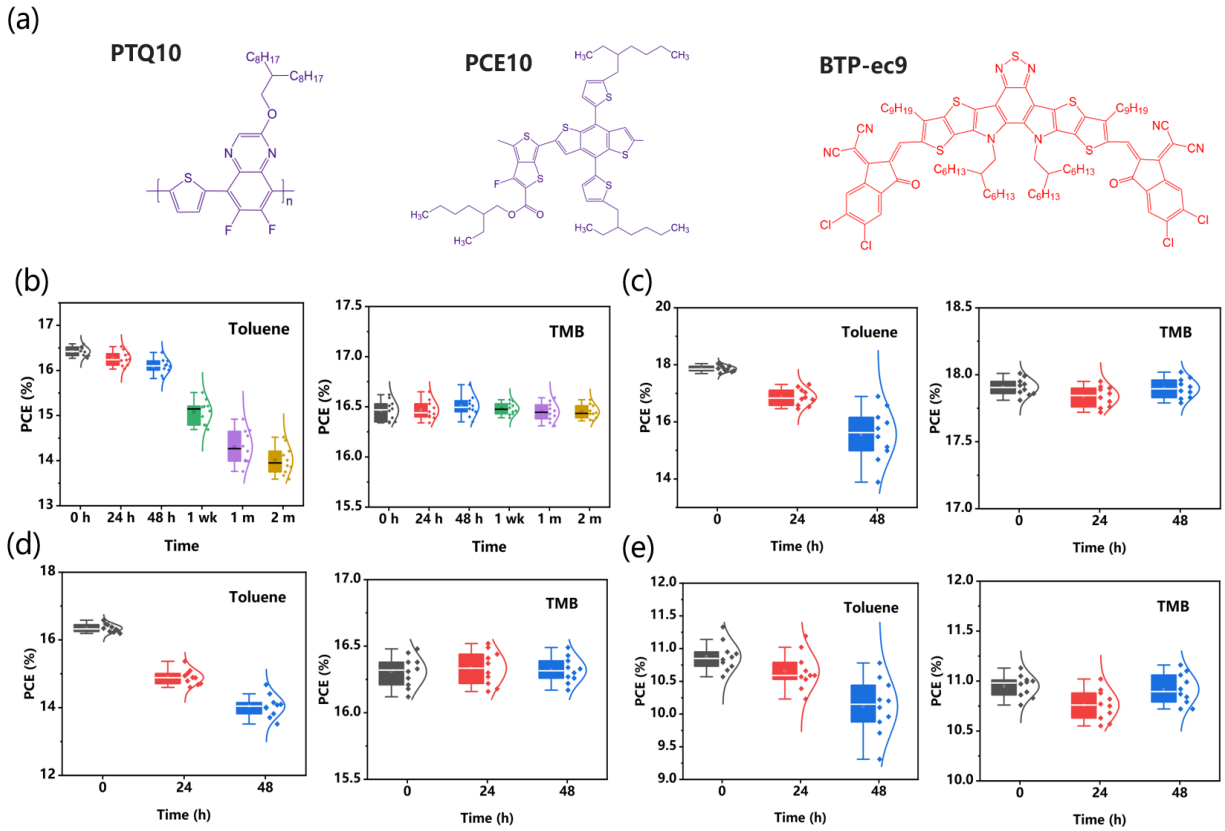

Fig.6 (a)The chemical structures of donor and acceptor and the PCE distributions for the (b) PM6/L8-BO devices with PM6 solutions at a concentration of 3 mg mL^{-1}, (c) PM6/L8-BO: BTP-ec9 devices, (d) PTQ10/L8-BO devices, and (e) PCEQ10/L8-BO devices.

determine the excellent storage stability in conjugated polymer solutions.

To make our research conclusion generalized, two other green solvents, o-Xylene and m-Xylene, were also used to investigate the stability of PM6 solution. First, we measured the polarity parameter $E_T(30)$ of two solvents, the chemical structures and the UV-Vis spectra for Reichardt's Dye in o-Xylene and m-Xylene are shown in Fig. S17. $E_T(30)$ values for o-Xylene and m-Xylene are 38.93 and 34.87 kcal mol^{-1}, respectively. The polarity parameters of the four solvents we studied, ranked from highest to lowest, are as follows: TMB (40.16 kcal mol^{-1}), o-Xylene, m-Xylene, Toluene (34.45 kcal mol^{-1}). The molar volumes of o-Xylene and m-Xylene are both 121.9 cm^3/mol, which lie between those of Toluene and TMB. The UV-vis absorption spectra of the PM6 solutions using o-Xylene and m-Xylene with different aging time were subsequently measured so as to analyze the aggregation degree. As shown in Fig. S18, when o-xylene is used as the solvent, there are no significant changes observed in the UV-vis absorption spectra, indicating the aggregation state in the solution is basically unchanged after aging. However, the H-type aggregation of PM6 in the m-xylene solution increases after aging according to the ratio of the 0-1 to 0-0 peaks and the slight redshift of the absorption peak, indicating an enhancement of the aggregation of PM6 molecule. Similarly, PM6/L8-BO OSCs using o-Xylene and m-Xylene as the solvents of PM6 solutions with different aging time were fabricated. The *J-V* curves and specific photovoltaic parameters of PM6/L8-BO devices are shown in Fig. S19a, b and Table S11, ESI. It can be observed that when o-Xylene is used as the solvent, the device efficiency remains essentially unchanged with prolonged solution aging time (~16.8%). However, when m-Xylene is used as the solvent, the device efficiency gradually decreases as the aging time increases (from 16.94% to 15.57% and then to 14.98%). This aligns with our conclusion that the larger polarity parameter of o-Xylene contributes to better stability of the solution, which is also reflected in the device efficiency. Furthermore, PTQ10/L8-BO OSCs using o-Xylene and m-Xylene were also fabricated to investigate whether the same trend can be observed. The *J-V* curves and specific photovoltaic parameters of PTQ10/L8-BO devices are shown in Fig. S19c, d and Table S12, ESI. The device performances indicate that as the solution aging time increases, PCE remains unchanged when o-Xylene is used as the solvent (~16.2%), whereas it decreases when m-Xylene is used as the solvent (from 16.28% to 15.78% and then to 13.73%). This observation is consistent with the phenomenon we observed in PM6/L8-BO OSCs, demonstrating that the influence of solvent polarity on solution stability and device performance exhibits a certain degree of universality in the field of OSCs.

Conclusion

In conclusion, we observed that the utilization of TMB as the solvent can generally enhance the solution stability of conjugated polymers. Due to the relatively bigger solvent polarity and molar volume, the TMB-based PM6 solutions could

maintain the stable storage state for up to 60 days. In Toluene based solution, the self-aggregation of PM6 molecules increases during aging, resulting in poor solution stability. We observed a declined PCE in the Toluene-processed devices after solution aging, accompanied by the deterioration of charge transport and a more dispersed PCE distribution. While all the device parameters remain stable after solution aging when using TMB solvent, demonstrating that the improvement of solution stability plays a significant role in maintaining the PCE of devices. The primary reason for the decreased device performance was found to be the reduced film uniformity coupled with the inappropriate phase separation within the film when using Toluene as the solvent. This work provides the scientific guidance on addressing the solution stability issues in terms of solvent selection pertinent to the commercial applications of OSCs, which facilitates the preparation, storage, and processing of the active layer solutions.

Author contributions

K. Z. conceived and designed the research. W. M. did the supervision. Y. C. performs the experiments, including device fabrication and characterizations, viscosity test, film morphology characterization and in-situ morphology characterizations. Z. Z. and H. Z. run the DFT calculation. W. M., N. J. and G. M. analyzed the experiment results. Y. C. drafted the manuscript. K. Z., H. Z., N. J., G. M. and W. M. revised the manuscript.

Conflicts of interest

There are no conflicts to declare.

Data availability

The data supporting the findings of this study are available within the article and its ESI.

Acknowledgements

Thanks for the support from the National Key Research and Development Program of China (2022YFE0132400), the National Natural Science Foundation of China (52173023, W2411049), and 111 project 2.0 (BP0618008). X-ray data was acquired at beamlines 7.3.3 and 11.0.1.2 at the Advanced Light Source, which is supported by the Director, Office of Science, Office of Basic Energy Sciences, of the U.S. Department of Energy under Contract No. DE-AC02-05CH11231. The authors thank Dr. Eric Schaible and Dr. Chenhui Zhu at beamline 7.3.3, and Dr. Cheng Wang at beamline 11.0.1.2 for assistance with data acquisition.

References

1 G. Zhang, F. R. Lin, F. Qi, T. Heumüller, A. Distler, H-J. Egelhaaf, N. Li, P. C. Y. Chow, C. J. Brabec, A. K.-Y. Jen, H-L. Yip, *Chem. Rev*., 2022, **122**, 14180-14274;

2 L. Zhu, M. Zhang, Z. Zhou, W. Zhong, T. Hao, S. Xu, R. Zeng, J. Zhuang, X. Xue, H. Jing, Y. Zhang, F. Liu, *Nat. Rev. Electr. Eng*., 2024, **1**, 581-596.

3 K. Liu, Y. Jiang, G. Ran, F. Liu, W. Zhang, X. Zhu, *Joule*, 2024, **8**, 835-851.

4 S. Guan, Y. Li, C. Xu, N. Yin, C. Xu, C. Wang, M. Wang, Y. Xu, Q. Chen, D. Wang, L. Zuo, H. Chen, *Adv. Mater*., 2024, **36,** 2400342.

5 L. Zhu, M. Zhang, G. Zhou, Z. Wang, W. Zhong, J. Zhuang, Z. Zhou, X. Gao, L. Kan, B. Hao, F. Han, R. Zeng, X. Xue, S. Xu, H. Jing, B. Xiao, H. Zhu, Y. Zhang, F. Liu, *Joule*, 2024, **8**, 3153-3168.

6 Y. Jiang, S. Sun, R. Xu, F. Liu, X. Miao, G. Ran, K. Liu, Y. Yi, W. Zhang, X. Zhu, *Nat. Energy*, 2024, **9,** 975-986.

7 Z. Zheng, J Wang, P. Bi, J. Ren, Y. Wang, Y. Yang, X. Liu, S. Zhang, J. Hou, *Joule*, 2022, **6**, 171-184.

8 L. Zhu, M. Zhang, J. Xu, C. Li, J. Yan, G. Zhou, W. Zhong, T. Hao, J. Song, X. Xue, Z. Zhou, R. Zeng, H. Zhu, C. Chen, R. C. I. MacKenzie, Y. Zou, J. Nelson, Y. Zhang, Y. Sun, F. Liu, *Nat. Mater*., 2022, **21**, 656-663.

9 Y. Sun, L. Wang, C. Guo, J. Xiao, C. Liu, C. Chen, W. Xia, Z. Gan, J. Cheng, J. Zhou, Z. Chen, J. Zhou, D. Liu, T. Wang, W. Li, *J. Am. Chem. Soc*., 2024, **146**, 12011-12019.

10 X. Zheng, Y. Wang, T. Chen, Y. Kong, X. Wu, C. Zhou, Q. Luo, C.-Q. Ma, L. Zuo, M. Shi, H. Chen, *FlexMat*, 2024, **1**, 221-233.

11 M. Kaltenbrunner, M.S. White, E.D. Głowacki, T. Sekitani, T. Someya, N.S. Sariciftci, S. Bauer, *Nat. Commun*., 2012, **3**, 770.

12 K. Fukuda, K. Yu, T. Someya, *Adv. Energy Mater*., 2020, **10**, 2000765,

13 Y. Li, G. Xu, C. Cui, Y. Li, *Adv. Energy Mater*., 2018, **8**, 1701791.

14 Y. Zhao, Z. Li, C. Deger, M. Wang, M. Peric, Y. Yin, D. Meng, W. Yang, X. Wang, Q. Xing, B. Chang, E. G. Scott, Y. Zhou, E. Zhang, R. Zheng, J. Bian, Y. Shi, I. Yavuz, K-H. Wei, K. N. Houk, Y. Yang, *Nat. Sustain*., 2023, **6**, 539-548.

15 S. Zou, Y. Shen, F. Xie, J. Chen, Y. Li, J. Tang, *Mater. Chem. Front*., 2020, **4**, 788-820.

16 S. Wang, J. Xu, W. Wang, G. N. Wang, R. Rastak, F. M. Lopez, J. W. Chung, S. Niu, V. R. Feig, J. Lopez, T. Lei, S. K. Kwon, Y. Kim, A. M. Foudeh, A. Ehrlich, A. Gasperini, Y. Yun, B. Murmann, J. B.-H. Tok, Z. Bao, *Nature*, 2018, **555**, 83-88.

17 Y. D. Park, H. S. Lee, Y. J. Choi, D. Kwak, J. H. Cho, S. Lee, K. Cho, *Adv. Funct. Mater*., 2009, **19**, 1200-1206.

18 M. Li, C. An, T. Marszalek, M. Baumgarten, H. Yan, K. Müllen, W. Pisula, *Adv. Mater*., 2016, **28**, 9430-9438.

19 Z. Xu, K. S. Park, J. J. Kwok, O. Lin, B. B. Patel, P. Kafle, D. W. Davies, Q. Chen, Y. Diao, *Adv. Mater*., 2022, **34**, 2203055.

20 M. M. Nahid, A. Welford, E. Gann, L. Thomsen, K. P. Sharma, C. R. McNeill, *Adv. Electron. Mater*., 2018, **4**, 1700559.

21 A. Khasbaatar, Z. Xu, J. H. Lee, G. C. Alvarado, C. H. Hwang, B. N. Onusaitis, Y. Diao, *Chem. Rev*., 2023, **123**, 8395-8487.

22 C. Guo, D. Li, L. Wang, B. Du, Z. Liu, Z. Shen, P. Wang, X. Zhang, J. Cai, S. Cheng, C. Yu, H. Wang, D. Liu, C. Li, T. Wang, *Adv. Energy Mater*., 2021, **11**, 2102000.

23 X. Xu, L. Yu, H. Yan, R. Li, Q. Peng, Energy Environ. Sci., 2020, 13, 4381-4388.

24 Y. Qin, L. Ye, S. Zhang, J. Zhu, B. Yang, H. Ade, J. Hou, *J. Mater. Chem. A*, 2018, **6**, 4324-4330.

25 T. Liu, J. Heimonen, Q. Zhang, C. Yang, J. Huang, H. Wu, M-A. Stoeckel, T. P. A. van der Pol, Y. Li, S. Y. Jeong, A. Marks, X. Wang, Y. Puttisong, A. Y. Shimolo, X. Liu, S. Zhang, Q. Li, M. Massetti, W. M. Chen, H. Y. Woo, J. Pei, I. McCulloch, F. Gao, M. Fahlman, R. Kroon, S. Fabiano, *Nat. Commun*., 2023, **14**, 8454.

26 R. Sun, T. Wang, X. Yang, Y. Wu, Y. Wang, Q. Wu, M. Zhang, C. J. Brabec, Y. Li, J. Min, *Nat. Energy*, 2022, **7**, 1087-1099.

27 Y. Zheng, Z. Yao, T. Lei, J. Dou, C. Yang, L. Zou, X. Meng, W. Ma, J. Wang, J. Pei, *Adv. Mater*., 2017, **29**, 1701072.
28 Z. Yao, J. Wang, J. Pei, *Prog. Polym. Sci*., 2023, **136**, 101626.
29 J. Rivnay, R. Noriega, R. J. Kline, A. Salleo, M. F. Toney, *Phys. Rev. B*, 2011, **84**, 045203.
30 D. M. Smilgies, *J. Appl. Crystallogr*., 2009, **42**, 1030-1034.
31 D. Leman, M. A. Kelly, S. Ness, S. Engmann, A. Herzing, C. Snyder, H. W. Ro, R. J. Kline, D. M. Delongchamp, L. J. Richter, *Macromolecules*, 2015, **48**, 383.
32 Z. Peng, L. Ye, H. Ade, *Mater. Horiz*., 2022, **9**, 577.
33 C. Reichardt, *Pure Appl. Chem*., 2008, **80**, 1415-1432.
34 H. Langhals, *Chem. Heterocycl. Compd*., 2017, **53**, 2-10.
35 V. G. Machado, R. I. Stock, C. Reichardt, *Chem. Rev*., 2014, **114**, 10429-10475.
36 P. Urbánek, I. Kuřitka, J. Ševčík, J. Toušková, J. Toušek, V. Nádaždy, P. Nádaždy, K. Végsö, P. Šiffalovič, R. Rutsch, M. Urbánek, *Polymer*, 2019, **169**, 243.
37 M. Lenes, M. Morana, C. J. Brabec, P. W. M. Blom, *Adv. Funct. Mater*., 2009, **19**, 1106.
38 V. D. Mihailetchi, L. J. A. Koster, J. C. Hummelen, P. W. M. Blom, *Phys. Rev. Lett*., 2004, **93**, 216601.
39 L. J. A. Koster, V. D. Mihailetchi, H. Xie, P. W. M. Blom, *Appl. Phys. Lett*., 2005, **87**, 203502.
40 P. N. Murgatroyd, *J. Phys. D. Appl. Phys*., 1970, **3**, 151-156.
41 V. D. Mihailetchi, J. Wildeman, P. W. Blom, *Phys. Rev. Lett*., 2005, **94**, 126602.
42 S. Engmann, F. A. Bokel, H. W. Ro, D. M. DeLongchamp, L. J. Richter, *Adv. Energy Mater*., 2016, **6**, 1502011.
43 J. Xue, H. Zhao, B. Lin, Y. Wang, Q. Zhu, G. Lu, B. Wu, Z. Bi, X. Zhou, C. Zhao, G. Lu, K. Zhou, W. Ma, *Adv. Mater*., 2022, **24**, 2202259.

The data supporting the findings of this study are available within the article and its ESI.